Title

Diffusion-Weighted Magnetic Resonance Imaging Characterization of White Matter Injury Produced by Axon-Sparing Demyelination and Severe Contusion Spinal Cord Injury in Rats

Journal

Journal of Neurotrauma, 33(10)

ISSN

0897-7151

Authors

Talbott, Jason F
Nout-Lomas, Yvette S
Wendland, Michael F
et al.

Publication Date

2016-05-15

DOI

10.1089/neu.2015.4102

Peer reviewed

JOURNAL OF NEUROTRAUMA 33:929–942 (May 15, 2016)

DOI: 10.1089/neu.2015.4102

Diffusion-Weighted Magnetic Resonance Imaging Characterization of White Matter Injury Produced by Axon-Sparing Demyelination and Severe Contusion Spinal Cord Injury in Rats

Jason F. Talbott,[1,4] Yvette S. Nout-Lomas,[2] Michael F. Wendland,[1] Pratik Mukherjee,[1,4] J. Russell Huie,[3,4] Christopher P. Hess,[1] Marc C. Mabray,[1] Jacqueline C. Bresnahan,[3,4] and Michael S. Beattie[3,4]

Abstract

Alterations in magnetic resonance imaging (MRI)–derived measurements of water diffusion parallel (D||) and perpendicular (D⊥) to white matter tracts have been specifically attributed to pathology of axons and myelin, respectively. We test the hypothesis that directional diffusion measurements can distinguish between axon-sparing chemical demyelination and severe contusion spinal cord white matter injury. Adult rats received either unilateral ethidium bromide (EB) microinjections (chemical demyelination) into the lateral funiculus of the spinal cord at C5 or were subjected to unilateral severe contusion spinal cord injury (SCI). Diffusion MRI metrics in the lateral funiculus were analyzed at early and late time-points following injury and correlated with histology. Early EB-demyelination resulted in a significant elevation in D⊥ and significant reduction in D|| at the injury epicenter, with histological evidence of uniform axon preservation. Alterations in D⊥ and D|| at the epicenter of early EB-demyelination were not significantly different from those observed with severe contusion at the epicenter, where histology demonstrated severe combined axonal and myelin injury. Diffusion abnormalities away from the injury epicenter were seen with contusion injury, but not with EB-demyelination. Chronic EB lesions underwent endogenous remyelination with normalization of diffusion metrics, whereas chronic contusion resulted in persistently altered diffusivities. In the early setting, directional diffusion measurements at the injury epicenter associated with chemical demyelination are indistinguishable from those seen with severe contusive SCI, despite dramatic pathologic differences between injury models. Caution is advised in interpretation of diffusion metrics with respect to specific white matter structural alterations. Diffusion analysis should not be limited to the epicenter of focal spinal lesions as alterations marginal to the epicenter are useful for assessing the nature of focal white matter injury.

Key words: contusion; demyelination; diffusion; diffusivity; MRI; spinal cord injury

Introduction

In clinical practice, magnetic resonance imaging (MRI) evaluation of the spinal cord for intramedullary pathology largely relies on conventional sequences, namely, qualitative description of T2 signal abnormality, identification of intramedullary hemorrhage, and gross morphologic distortions, such as spinal cord compression.[1] Conventional techniques are limited with respect to sensitivity, specificity, and prognostic capacity for spinal cord injury (SCI) patients.[1]

Diffusion-weighted MRI techniques, including diffusion tensor imaging (DTI), characterize the diffusive motion of water molecules in tissues.[2] The highly organized architecture of spinal cord white matter, with a large predominance of axons oriented parallel to the long axis of the spinal cord, results in highly anisotropic diffusion of water along the major spinal cord axis, rendering diffusion imaging an excellent probe for interrogating spinal cord white matter integrity.[3–5] Compared with conventional MRI sequences, diffusion MRI has demonstrated increased sensitivity for detection of white matter pathology in the spinal cord.[5–9]

[1]Department of Radiology and Biomedical Imaging, San Francisco General Hospital and University of California, San Francisco, San Francisco, California.
[2]College of Veterinary Medicine and Biomedical Sciences, Colorado State University, Fort Collins, Colorado.
[3]Department of Neurological Surgery, University of California, San Francisco, San Francisco, California.
[4]Brain and Spinal Injury Center, San Francisco General Hospital, San Francisco, California.

Moreover, diffusion MRI-derived quantitative parameters reflecting directional diffusivity of water have been shown to reflect specific white matter pathologic processes.[10–14]

For example, radial diffusivity (symbolically denoted as $\lambda\perp$ when calculated as the average of the second and third eigenvalues of the diffusion tensor, or $D\perp$ when measured as the apparent diffusion coefficient [ADC] with the diffusion gradient orientation perpendicular to the long axis of the spinal cord), quantifies water diffusion perpendicular to the major axis of white matter axon bundles and has been shown to be a biomarker of myelin pathology.[12] Axial diffusivity (symbolically denoted as $\lambda\|$ when calculated as the first eigenvalue of the diffusion tensor, or $D\|$ when measured as the ADC when the gradient orientation is parallel to the long axis of the spinal cord) quantifies water diffusivity parallel to the long axis of axon bundles and has been shown to serve as a biomarker of axonal pathology.[11,12,15] An anisotropy index (AI) derived from these measures (or fractional anisotropy with DTI) provides a quantitative measure for the degree of directionally-limited (i.e., anisotropic) water diffusion in tissue. Thus, *in vivo* diffusion MRI has demonstrated potential as a quantitative biomarker for axon and myelin integrity that may greatly facilitate diagnosis and prognosis for a variety of spinal cord pathologies.[16]

One limitation to previous studies attributing MRI diffusion parameters to specific white matter pathology relates to the nature of injury models utilized. Pre-clinical studies first attributing $\lambda\perp$ and $\lambda\|$ to myelinopathy and axonopathy utilized genetic models of dysmyelination,[11] which do not accurately reflect acquired demyelinating injuries more commonly seen in adults. Complex inflammatory, traumatic, and ischemic white matter injury models, wherein axon and myelin pathology co-exist, were subsequently studied.[12,14,15,17–19] Concomitant inflammatory activation, gliosis, vasogenic edema, and cytotoxic injury associated with these injury models complicate interpretation of the pathologic specificity of $\lambda\perp$ and $\lambda\|$.[20, 21] Moreover, these complex injury models rely upon correlation analysis of diffusion metrics, with immunohistochemical (IHC) or histologic markers following inexact registration of relatively low resolution MRI images, compared with ultra-high resolution histologic/IHC images.

Simpler *in vivo* white matter injury models, with more homogenous and isolated demyelinating pathology, may better demonstrate the specificity of directional diffusion indices for myelinopathy *in vivo.* Ethidium bromide (EB)–induced demyelination is a well characterized glial toxic model of chemical demyelination most commonly induced by direct microinjection of EB into targeted white matter tracts.[22,23] Resultant astrocyte and oligodendrocyte cell death secondary to the DNA intercalating properties of EB results in a uniform field of demyelination, with preservation of denuded axons within approximately 7 days of toxin injection.[23,24] In rat models, subsequent remyelination of EB lesions by endogenous precursor cells occurs in a stereotypic fashion within 3–6 weeks of injection.[23] Thus, EB-induced demyelination is a focal, highly reproducible, and predictable injury model for studying demyelination and remyelination without significant secondary axonal disruption or primary inflammatory response.

In the present study, we sought to quantify the longitudinal ($D\|$), transverse ($D\perp$), and resulting AI values following focal EB demyelination of the lateral funiculus of the rat cervical spinal cord during the early phase of injury, when there is maximal demyelination, as well as during the chronic stage, when complete endogenous remyelination has occurred. Further, we compared these measurements with a severe hemi-contusion injury, which is ablative to both myelin and axons. We hypothesized that patterns of $D\|$ and $D\perp$ alterations will distinguish between these two distinct injury models during the early and chronic phases of injury.

Methods

Animal subjects

A total of 26 female Sprague-Dawley rats (Charles River Laboratories, Hollister, CA) were used for this study, age 84 days (range 83–86 days) at the initiation. Rats were housed individually in cages and maintained on a 12-h light/dark cycle. All animals had *ad libitum* access to food and water. All animal experiments were conducted after approval by the Institutional Laboratory Animal Care and Use Committee of University of California, San Francisco, and were performed in compliance with National Institutes of Health (NIH) guidelines and recommendations.

Animal surgery procedures and post-operative care

Surgeries were performed with aseptic technique under deep anesthesia induced and maintained by inhalation of isoflurane (IsoFlow; Abbott Laboratories, North Chicago, IL; 2–3%). Anesthetic plane was assessed with foot pinch. Lacrilube ophthalmic ointment (Allergan Pharmaceuticals, Irvine, CA) was applied to the eyes before surgery. Body temperature monitoring during surgery was performed with a rectal thermal probe and maintained at 37.5°C using a heating pad.

EB injection. Following induction of anesthesia, dorsal laminectomies were performed at the C4-C5 vertebral levels. The dura was carefully opened transversely at two sites 2 mm apart along the craniocaudal axis. Unilateral stereotactic injection (1 uL/injection at each coordinate depth) of 0.1 mg/mL EB was delivered at pre-defined coordinates targeting the lateral funiculus (1.2 mm lateral to midline and depths of 0.9 and 1.2-mm) at two separate craniocaudal locations 2 mm apart based on stereotactic coordinates derived from a rat neuroanatomical atlas. EB injections were performed using custom-pulled and beveled glass micropipettes attached to a picospritzer.[24,25] The wound was closed in anatomical layers and analgesic (buprenorphine, 0.05 mg/kg [Buprenex]; Hospira, Inc., Lake Forest, IL) along with antibiotic (Cefazolin, 50 mg/kg; Henry Schein, Melville, NY) were administered.

Cervical hemi-contusion. Following induction of anesthesia, dorsal laminectomy was performed at C5. Unilateral 100 kdyne contusion injuries were produced using the Infinite Horizon Impactor (Precision Systems and Instrumentation LLC, Fairfax, VA) with a modified impactor tip 2 mm in diameter. Injury severity was severe (100 kilodynes). Wound closure and postoperative care were performed as for EB surgeries.

In vivo *MRI*

In vivo MRI was performed using a 7 Tesla Varian narrow-bore MRI system (Varian Medical Systems, Inc., Palo Alto, CA) with 60 mT/m gradient insert. A custom-made receiver coil designed for the rat cervical spine was used. All MRI was performed with respiratory gating. Scout images were obtained to confirm alignment of the cervical spinal cord reference frame (from C2-C7 vertebral segments) with the MRI reference frame. In some cases, padding was placed along the ventral aspect of the neck to straighten the cervical lordosis and align the spinal cord with the magnetic reference frame. For diffusion-weighted imaging, a Stejskal-Tanner spin-echo multi-slice sequence with gradients applied in three separate orthogonal orientations matching the ''x'' (1, 0, 0), ''y'' (0, 1, 0), and ''z'' (0, 0, 1) axes of the main magnetic field were performed. A b value of approximately 890 sec/mm2 was applied

for diffusion in the ''x'' and ''y'' planes, while a b value of approximately 400 sec/mm^2 was used in the ''z'' plane. Lower b value in the ''z'' axis was used to maintain signal-to-noise ratio. A T2-weighted sequence with no gradient application served as the B0 image (0, 0, 0). Additional imaging parameters included a repetition time = ~2000 msec (variable, dependent upon respiratory rate), echo time = 35 msec, and field of view = 2.56 cm^2, with 128 × 128 matrix for in-plane resolution of 200 μm. Slice thickness was 1.5 mm.

ADC values in the longitudinal (D$\|$) and transverse (D$\perp$) gradient directions were calculated based on the degree of signal attenuation of the diffusion-weighted sequence, compared with the B0 sequence, according to the mono-exponential equation (1)

$$D = \frac{\mathrm{In}\left[\frac{S_0(b)}{S_n(b)}\right]}{b}$$

where D = apparent diffusion coefficient, S0 = signal without diffusion-sensitizing gradients (b = 0), Sn = signal with diffusion sensitizing gradient applied, and b = b value. D$\|$ was calculated directly from gradients applied in the ''z'' axis while D$\perp$ was calculated as the mean average of ADC with gradients applied in the ''x'' and ''y'' planes (D$\perp$ = [Dx + Dy]/2). As previously described,[26] an AI based on directional ADCs was derived according to equation (2)

$$AI = \frac{D\,\| - D\,\perp}{D\,\| + D\,\perp}$$

For acute EB lesions, manual region-of-interest (ROI) was drawn to approximate the area of T2-weighted signal hyperintensity in the lateral funiculus at the injury epicenter as identified on the B0 and diffusion-weighted image with longitudinal gradient orientation (z-axis; Fig. 1). ROI analysis at levels cranial and caudal to the injury epicenter were selected to match the location in the transverse cord plane of epicenter signal abnormality, with utilization of identical sized ROI used at the epicenter. For chronic EB lesions, no appreciable residual T2 hyperintensity was evident in any animal; therefore, ROIs were selected at the level of the laminectomy at the stereotactic targeted sites.

For the hemi-contusion lesion, similar sized ROI as utilized for EB lesions were used to sample T2-hyperintense regions of the lateral funiculus at the injury epicenter. Care was taken to not include regions of T2-hypointense signal (which was largely confined to gray matter) in the ROI so as not to sample hemorrhagic regions that may interfere with diffusion analysis. Control diffusion measurements of lateral funiculus white matter was measured in the EB lesion animals, contralateral to the side of EB injection (n = 10). To confirm the validity of these internal control measurements, D$\|$ and D$\perp$ were measured in the bilateral lateral funiculi of three naïve age-matched rats. Imaging from one of these animals was used for the creation of Figure 1. Quantitative measurements of the EB and hemi-contusion injury dimensions were manually obtained on the T2-weighted B0 sequence. Volumes were calculated by the formula for approximate ellipse volume = (π/6)*length*width*-height. All image post-processing was performed with ImageJ software (ImageJ; NIH, Bethesda, MA). Motion correction between sequences was manually performed using the translation function in ImageJ software platform prior to diffusion analysis.

Tissue processing

Animals were sacrificed at 7 (n = 10), or 65 (n = 5) days post-injury (dpi) for EB demyelination and 3 (n = 5) or 65 (n = 3) dpi for

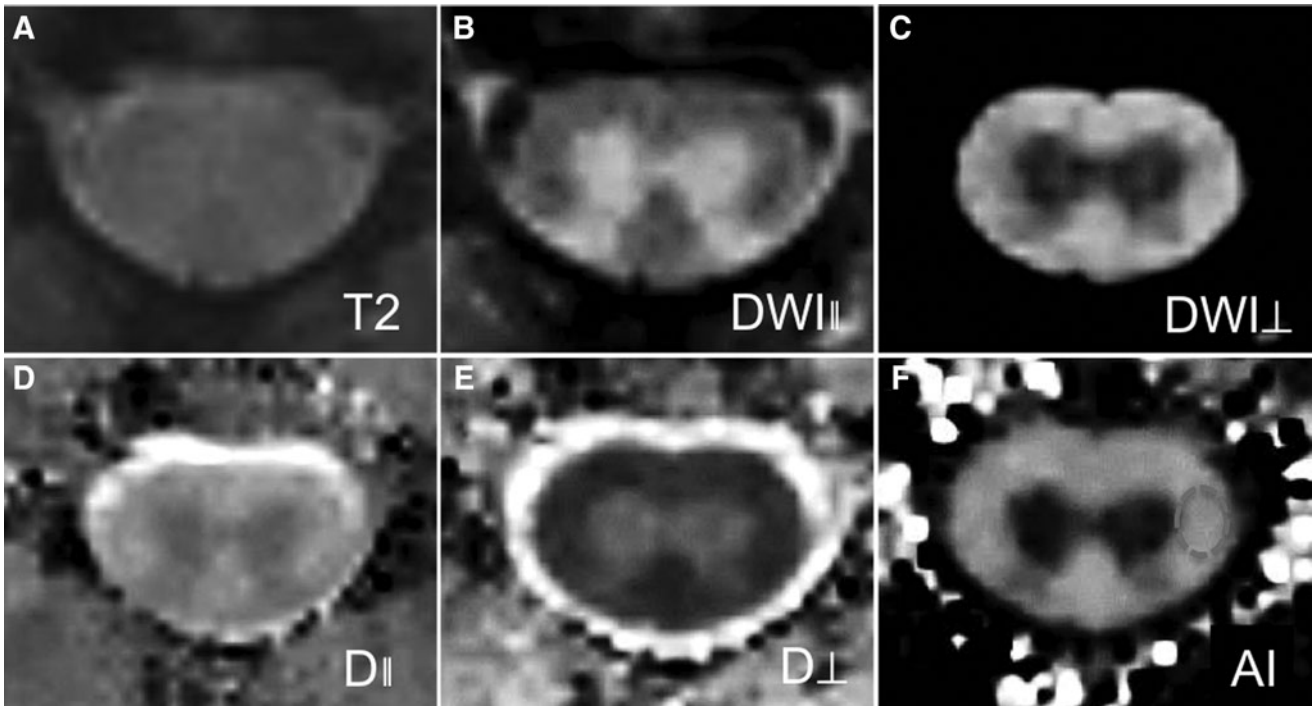

FIG. 1. *In vivo* diffusion magnetic resonance imaging of the normal adult rat cervical spinal cord. Axial T2 **(A)**, DWI-$\|$ **(B)**, and DWI-$\perp$ **(C)** images are shown with excellent gray–white matter contrast appreciated on the diffusion-weighted images. Calculated ADC maps for D$\|$ **(D)**, D$\perp$ **(E)**, and AI **(F)** at the same level also are shown. Dashed oval in F approximates the area of the lateral funiculus sampled for measurements in control and injury models. DWI-$\|$, longitudinal diffusion-weighted image; DWI-$\perp$, transverse diffusion-weighted image; ADC, apparent diffusion coefficient; D$\|$, longitudinal apparent diffusion coefficient; D$\perp$, transverse apparent diffusion coefficient; AI, anisotropy.

contusion SCI. Tissue processing was as previously described.[24] Briefly, animals were deeply anesthetized with sodium pentobarbital (60 mg/kg) and transcardially perfused with 100 mL of 0.1 M phosphate-buffered saline (PBS) followed by 300 mL of 4% paraformaldehyde in 0.1 M PBS. Spinal cords were carefully dissected and post-fixed overnight at 4°C, then transferred to 30% sucrose at 4°C for cryoprotection (48 h). Specimens were cut transversely at the epicenter of the lesion and mounted with cut surfaces facing down in Tris-buffered saline (TBS) tissue freezing medium (Triangle Biomedical Sciences, Durham, NC).

Immunohistochemistry and fluorescence microscopy

After tissue embedding, 20-μm thick transverse sections were cut on a cryostat device and mounted on microscope slides. Before incubation with primary antibodies, sections were permeabilized and blocked with 0.3% Triton X-100/10% normal donkey serum in 0.1 M TBS (pH = 7.4) for 30 min. Primary antibodies were then applied for 48 h at 4°C. The following primary antibodies were used: anti-myelin basic protein (1:20; Sigma-Aldrich, St. Louis, MO) for intact myelin, anti-phosphorylated neurofilament H (1:300, SMI-31-Sternberger Monoclonals, Lutherville, MD) for intact axons, anti-βAPP (1:200; Chemicon Inc., Temecula, CA) for damaged axons, anti- glial fibrillary acidic protein (GFAP; 1:200; Dako, Cupertino, CA) for astrocytes, and anti-degMBP (1:800; Chemicon Inc.) for degenerated myelin. Appropriate secondary antibodies were used. Sections were then rinsed in TBS and cover-slipped with antiface mounting media (Molecular Probes, Eugene, OR). Staining was visualized with a Keyence BZ-900 all-in-one fluorescence microscope with built-in monochrome CCD camera (Keyence Corporation, Itasca, IL). Figures were assembled using ImageJ and Adobe Photoshop software (San Jose, CA).

Histological analysis

Histological analysis was performed on 1-μm thick plastic toluidine blue–stained sections as previously described.[24] For luxol fast blue (LFB) staining, cryostat sections were dehydrated in graded alcohol and placed in 0.1% LFB at 37°C overnight. Sections were then differentiated in 0.05% $LiCO_3$ for 4 min, dehydrated in graded alcohol and xylene, and cover-slipped.

Axon density was quantified for acute EB lesions based on density of SMI-31$^+$ axon counts. Cryostat sections from the epicenter of early EB lesions from three different animals were analyzed. Digitized images of the lesion, as well as areas of normal contralateral spinal cord, were obtained at 40× magnification. Axon density within the lesion and contralateral normal spinal cord was assessed by manually counting the total number of SMI-31$^+$ axons in a 60 μm × 60 μm square. Five squares were randomly sampled per section. Results are reported as axons/mm^2.

Statistical analysis

Statistical analysis was performed using MedCalc for Windows, version 14.8.1 (MedCalc Software, Ostend, Belgium). One-way analysis of variance (ANOVA) was performed for lesion volume, D$\|$, D$\perp$, and AI at each location to assess differences between groups. As part of ANOVA, a Levene's test was performed to assess for a normal distribution and if necessary, the data was log-transformed to achieve a normal distribution for analysis. If the ANOVA was statistically significant then Tukey-Kramer pairwise comparisons were performed. In order to keep an overall study alpha of 0.05, a Bonferroni *post hoc* correction was applied to the ANOVAs and the *t*-test, requiring a $p < 0.003125$ for statistical significance. A $p < 0.05$ was considered statistically significant for Tukey-Kramer tests within a statistically significant ANOVA as these tests account for multiple comparisons. For quantitative axon density analysis, a two-tailed Student's *t*-test was used to compare measurements of axon density in early EB and normal white matter samples. A $p < 0.05$ was considered statistically significant.

Results

MRI of the normal rat cervical spinal cord

Representative *in vivo* T2-weighted and diffusion-weighted MRI images, along with calculated directional ADC (D$\|$ and D$\perp$) and AI maps of the rat cervical spinal cord, are shown in Figure 1. The uninjured lateral funiculus demonstrated an average D$\| = 2.62 \times 10^{-3}$ mm^2/msec ($\pm$ 0.7×10^{-3} mm^2/msec), average D$\perp = 0.29 \times 10^{-3}$ mm^2/msec ($\pm$ 0.029 mm^2/msec), with resulting average AI = 0.8. D$\|$ and D$\perp$ also were measured in the bilateral lateral funiculi of three naïve age-matched control rats (total of six measurements for each parameter) with measurements of 0.3×10^{-3} mm^2/msec ($\pm$ 0.02×10^{-3} mm^2/msec; $p = 0.15$ for comparison with internal control) and 2.69×10^{-3} mm^2/msec ($\pm$ 0.79×10^{-3} mm^2/msec; $p = 0.79$ for comparison with internal control), respectively. Because these measurements were not significantly different from our internal control measurements, the internal controls values were used for all subsequent comparisons.

Acute EB lesions demonstrate uniform demyelination in the lateral funiculus with preservation of axons

Consistent with prior literature,[23] injection of EB into the lateral funiculus resulted in a characteristic demyelinating injury with preservation of axons as evidenced by toluidine blue staining and SMI-31/βAPP immunohistochemistry (Fig. 2). At 7 dpi, swaths of demyelinated axons were observed within the lesion epicenter with irregular myelin basic protein (MBP) staining for normal myelin and extensive positive staining for degenerated MBP, consistent with myelin debris (Fig. 2). No significant quantity of normally myelinated axons were observed within the early EB lesion epicenter, although occasional incompletely demyelinated axons were present. SMI-31$^+$ staining for intact axons was seen within acute EB lesions, without appreciable staining for βAPP, a marker of damaged axons (Fig. 2), consistent with axonal preservation. Quantitative axon densities based on SMI-31$^+$ immunohistochemistry showed that axon densities within early EB lesions (5796 axons/mm^2 $\pm$ 733) were not significantly different from normal white matter (5759 axons/mm^2 $\pm$ 607; $p = 0.88$). In addition to demyelination, EB lesions are largely devoid of astrocytes as evidenced by lack of GFAP staining within the lesion (Fig. 2).

T2-weighted MRI of the epicenter of acute EB and acute hemi-contusion injuries

During the early phase (7 dpi), EB injection consistently resulted in a well-circumscribed ellipsoid T2-hyperintense lesion confined to the lateral funiculus of the cervical spinal cord. No significant T2 hypointense signal was seen within the EB lesion to suggest hemorrhage. Average lesion dimensions based on T2-hyperintense signal abnormality are listed in Table 1, with average lesion volume of 1.66 mm^3 ($\pm$ 0.27 mm^3).

During the early phase of cervical hemi-contusion injury (3 dpi), intramedullary signal abnormality involving the entire hemi-cord at the lesion epicenter on axial T2 sequences was consistently seen (Fig. 3). Heterogeneous T2 signal abnormality was evident as previously described,[27,28] with a central core of T2 hypointense susceptibility artifact primarily confined to the spinal gray matter, corresponding to hemorrhage (Fig. 3). More extensive surrounding

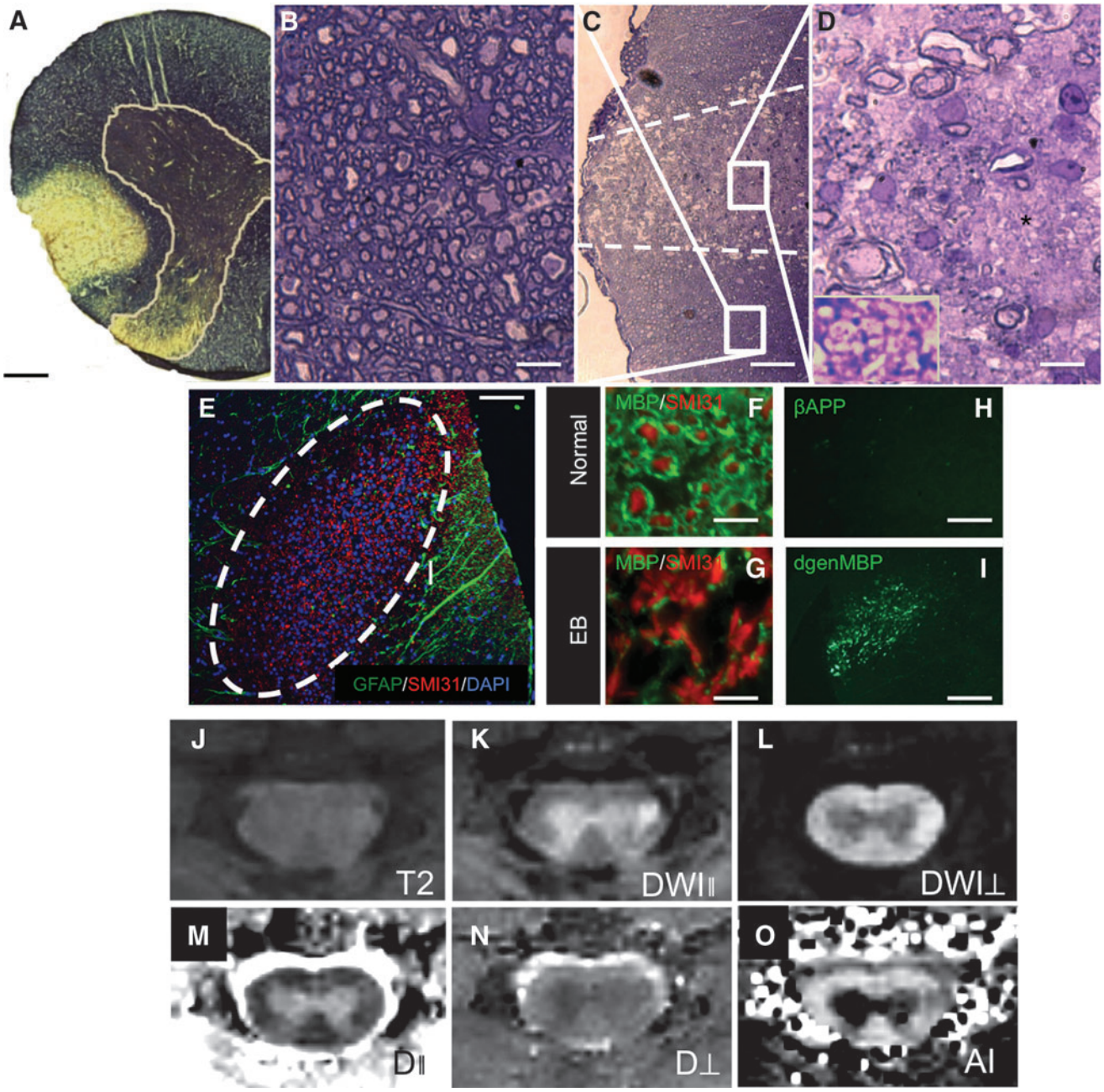

FIG. 2. Early EB demyelination results in uniform demyelination with preservation of axons and altered diffusion metrics. **(A)** Luxol fast blue stain for myelin shows uniform myelin pallor corresponding to site of EB injection into the lateral funiculus. Low (10×) magnification toluidine blue image **(C)** of the lateral funiculus shows the region of EB demyelination. Coned-in higher magnification (40×) views of adjacent normal white matter **(B)** and EB lesion **(D)** demonstrates the histological contrast with EB lesions consisting of fields of demyelinated axons and myelin debris. Left lower inset in (D) shows digitally magnified view of demyelinated axons profiles in region of black asterisk. Immunohistochemistry (IHC) for $GFAP^+$ astrocytes and $SMI31^+$ axons **(E)** shows ablation of astrocytes within the lesion (lesion outlined in white dashed oval in E). MBP and SMI-31 IHC in spared white mater **(F)** shows intact myelin rings enseathing axons, whereas this orientation is disrupted in EB lesions **(G)**. No appreciable staining for βAPP, a marker of damaged axons, is seen in EB lesions **(H)**, while extensive degenerated MBP staining is evident **(I)**. Axial T2- **(J)**, DWI-$\parallel$ **(K)**, and DWI-$\perp$ **(L)** weighted magnetic resonance imaging images along with calculated apparent diffusion coefficient maps for D$\parallel$ **(M)**, D$\perp$ **(N)**, and AI **(O)** show the EB lesion in the left lateral funiculus (best seen in K). Calculated AI map (O) shows the reduced anisotropy associated with early EB demyelination. EB, ethidium bromide; GFAP, glial fibrillary acidic protein; SMI-31, antibody against phosphorylated neurofiliament in axons; MBP, myelin basic protein; βAPP, amyloid beta precursor protein; DWI-$\parallel$, longitudinal diffusion-weighted image; DWI-$\perp$, transverse diffusion-weighted image, D$\parallel$, longitudinal apparent diffusion coefficient; D$\perp$, transverse apparent diffusion coefficient; AI, anisotropy index. Scale bar = 250 μm in A, 15 μm in C and 5 μm B and D. Color image is available online at www.liebertpub.com/neu

Table 1. Lesion Volume Measurements

	Lesion volume by MRI					
	Acute contusion (AC)	*Acute ethidium bromide (AEB)*	*Chronic contusion (CC)*	p *value from post-ANOVA pairwise comparisons*		
				AC vs. CC	*AEB vs. CC*	*AC vs. AEB*
Lesion volume in mm^3	14.405 ± 2.758	1.662 ± 0.272	0.886 ± 0.028	<0.01	<0.01	<0.01

ANOVA, $F = 342.836$; $p < 0.001$.
MRI, magnetic resonance imaging; ANOVA, analysis of variance.

T2 hyperintense signal involving virtually the entire dorsal column, and lateral and ventral funiculi of the ipsilateral spinal cord was seen at the epicenter with dimensions of signal abnormality as listed in Table 1. The average volume of intramedullary signal abnormality was 14.41 mm^3 ($\pm 2.76\ mm^3$); significantly larger than the EB lesion ($F = 342.836$; $p < 0.001$, pairwise $p < 0.01$).

Diffusion MRI at the epicenter of acute EB and acute hemi-contusion injuries

Diffusion measurements for early EB (7 dpi), and early hemi-contusion (3 dpi) injuries are listed in Table 2 and graphically displayed in Figure 4. One-way ANOVA demonstrated statistically

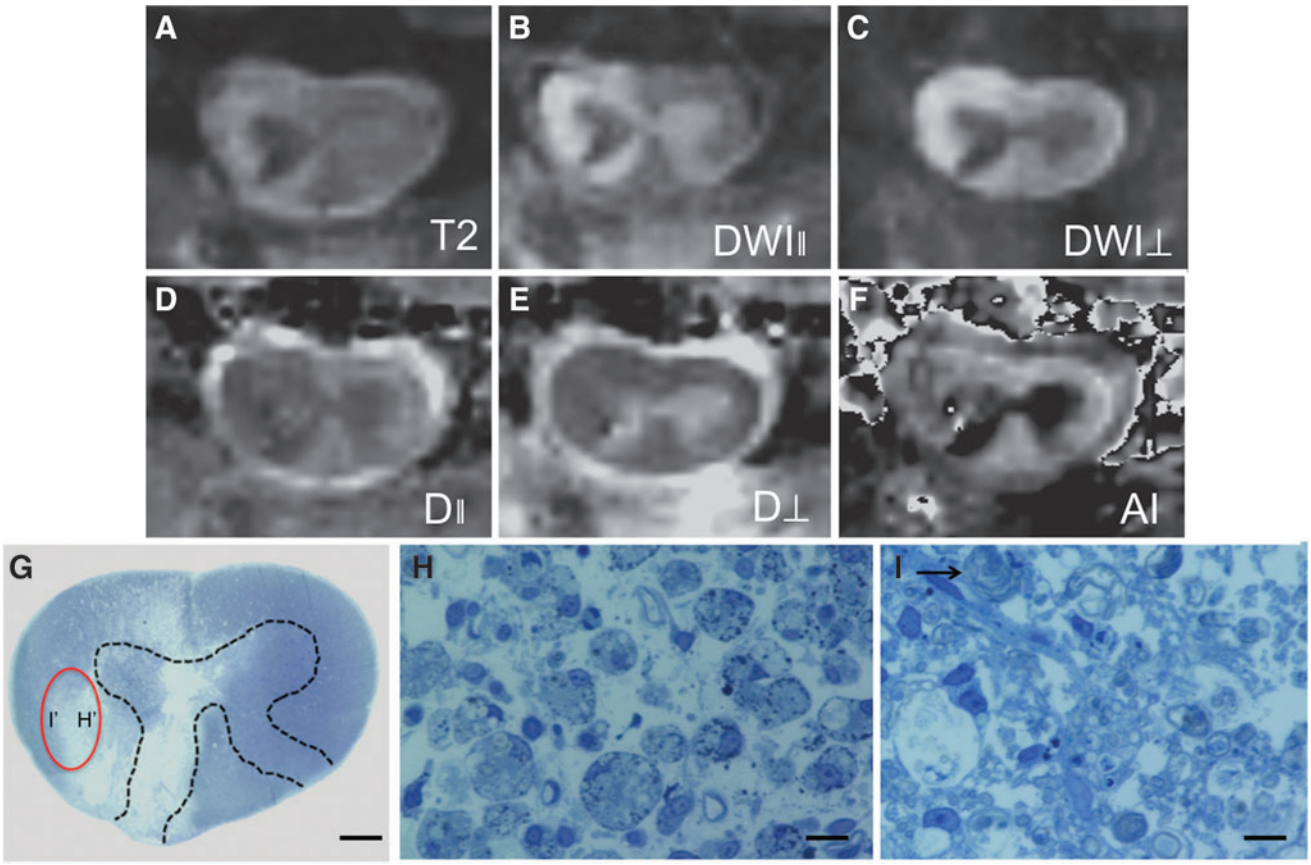

FIG. 3. Magnetic resonance imaging (MRI) and histology of early severe hemi-contusion SCI. *In vivo* axial T2-weighted **(A)**, DWI-|| **(B)**, and DWI-⊥ **(C)** MRI images along with calculated ADC maps for D|| **(D)**, D⊥ **(E)**, and AI **(F)** show extensive signal abnormality in the left hemi-cord 3 dpi. Hypointense signal primarily confined to ipsilateral gray matter corresponds to regions of confluent micro-hemorrhage. No gross hemorrhage is seen on MRI in the lateral funiculus and hemorrhagic regions were excluded from ROI analysis. Calculated AI map (F) shows the irregular reduced anisotropy associated with early severe contusion SCI. Toluidine blue stained semi-thin section at the epicenter of a representative hemi-contusion animal **(G)** shows extensive tissue distruction in the right hemi-cord. High magnification view (100×) of the medial aspect of the sampled lateral funiculus **(H)** is primarily composed of macrophages laden with myelin and axonal debris. The more peripheral margin of the sampled lateral funiculus **(I)** contains admixture of degenerating axons and unraveling myelin (black arrow in I) as well as scattered residual thinly myelinated small axons, macrophages, and reactive astrocytes. Red oval in G approximates the ROI selected for diffusion metric analysis. I′ and H′ in G approximate the location of high magnification images in panels H and I. SCI, spinal cord injury; DWI-||, longitudinal diffusion-weighted image; DWI-⊥, transverse diffusion-weighted image; D||, longitudinal apparent diffusion coefficient; D⊥, transverse apparent diffusion coefficient; dpi, days post-injury; ROI, region of interest; AI, anisotropy index. Scale bar = 300 μm in G, 10 μm in H and I. Color image is available online at www.liebertpub.com/neu

Table 2. Acute Injury Diffusion Metrics

		Early injury (3 and 7 dpi)					
					p *value from post-ANOVA pairwise comparisons*		
Region	*Measure*	*Acute contusion (AC)*	*Acute ethidium bromide (AEB)*	*Control (C)*	*AC vs. C*	*AEB vs. C*	*AC vs. AEB*
Cranial 6	$D_{\perp}$	0.291 ± 0.144	0.296 ± 0.064	0.294 ± 0.056	NS	NS	NS
	$D_{\parallel}$	1.983 ± 0.198	2.567 ± 0.403	2.620 ± 0.719	NS	NS	NS
	AI	0.769 ± 0.105	0.790 ± 0.053	0.802 ± 0.034	NS	NS	NS
Cranial 3	$D_{\perp}$	0.386 ± 0.087	0.289 ± 0.035	0.313 ± 0.060	NS	NS	NS
	$D_{\parallel}$	1.670 ± 0.199	2.950 ± 0.589	2.905 ± 0.774	<0.01	>0.05	<0.01
	AI	0.629 ± 0.067	0.813 ± 0.016	0.802 ± 0.009	<0.05	>0.05	<0.01
Epicenter	$D_{\perp}$	0.622 ± 0.154	0.662 ± 0.174	0.334 ± 0.030	<0.01	<0.01	>0.05
	$D_{\parallel}$	1.720 ± 0.447	1.692 ± 0.282	2.837 ± 0.782	<0.01	<0.01	>0.05
	AI	0.434 ± 0.152	0.451 ± 0.140	0.777 ± 0.060	<0.01	<0.01	>0.05
Caudal 3	$D_{\perp}$	0.643 ± 0.101	0.280 ± 0.051	0.329 ± 0.044	<0.01	>0.05	<0.01
	$D_{\parallel}$	1.665 ± 0.291	2.860 ± 0.669	2.808 ± 0.659	<0.01	>0.05	<0.01
	AI	0.459 ± 0.046	0.795 ± 0.025	0.782 ± 0.049	<0.01	>0.05	<0.01
Caudal 6	$D_{\perp}$	0.388 ± 0.159	0.295 ± 0.050	0.210 ± 0.068	NS	NS	NS
	$D_{\parallel}$	1.925 ± 0.608	2.512 ± 0.255	2.719 ± 0.481	NS	NS	NS
	AI	0.698 ± 0.063	0.787 ± 0.040	0.788 ± 0.041	>0.05	>0.05	>0.05

NS = non-significant ANOVA that did not go on to pairwise comparisons with a Tukey-Kramer *post hoc* test. dpi, days post-injury; ANOVA, analysis of variance; $D\perp$, magnetic resonance imaging (MRI)–derived measurements of water diffusion perpendicular to white matter tracts; $D\parallel$, MRI-derived measurements of water diffusion parallel to white matter tracts; AI, anisotropy index.

significant differences in $D\perp$ ($F = 35.430$; $p < 0.001$), $D\parallel$ ($F = 7.077$; $p = 0.001$), and AI ($F = 20.452$; $p < 0.001$) at the lesion epicenter for both EB and contusion injuries, compared with normal white matter. With both injuries, $D\parallel$ was significantly decreased ($p < 0.01$), $D\perp$ significantly elevated ($p < 0.01$), and AI significantly decreased ($p < 0.01$), compared with control. Neither $D\parallel$, $D\perp$, nor AI were significantly different ($p > 0.05$) between EB and hemi-contusion injuries at the level of the injury epicenter during the early phase of injury.

Acute contusion results in extensive injury to axons and myelin at the injury epicenter

Examination of toluidine blue–stained semi-thin sections interrogating the lateral funiculus at the contusion epicenter demonstrated extensive ablation of both axons and myelin, similar to prior reports for thoracic and cervical contusion injury.[29,30] Along the medial aspect of the lateral funiculus, no significant quantity of intact axons was observed and the damaged tissue was primarily composed of macrophages containing extensive myelin and axonal debris (Fig. 3). The more peripheral margins of the lateral funiculus were notable for an admixture of degenerating axons, active demyelination as well as macrophages and proliferating astrocytes on histologic sections. Occasional intact axons with variable myelin thickness were observed in the most peripheral margins of the lateral funiculus.

Histology, T2 and diffusion MRI of chronic EB and hemi-contusion injury epicenter

At the chronic time-point (65 dpi), EB lesions demonstrated extensive remyelination by a combination of oligodendrocytes and Schwann cells (Fig. 5). No appreciable residual T2 signal abnormality was seen within the spinal cord at the site of EB injection (Fig. 5). There was complete normalization of T2 signal, $D\parallel$, $D\perp$, and AI values for the chronic EB lesion (Fig. 5 and Table 3).

During the chronic stages of hemi-contusion injury, a T2-hyperintense cystic cavity was consistently identified in the region of the lateral frontal horn and lateral funiculus at the lesion epicenter (Fig. 6). Histological sections revealed intact peri-cavitary tissue in the peripheral lateral funiculus comprised of sparsely clustered axon fascicles, many of which were remyelinated by Schwann cells. Scattered macrophages, astrocytes, and fibrous interstitial tissue also were observed (Fig. 6). Average cavity dimensions based on T2-weighted imaging are reported in Table 1. Although no appreciable T2 signal abnormality was evident beyond the cystic cavity, asymmetric atrophy of the ipsilateral spinal cord was evident at the epicenter and several millimeters cranial and caudal to the cystic cavity on both MRI and histologic sections (Fig. 6). The epicenter of chronic hemi-contusion injuries demonstrated near isotropic diffusion values ($D\parallel = 2.67 \pm 0.22\ mm^2/msec$; $D\perp = 2.22 \pm 0.90\ mm^2/msec$; $AI = 0.12$), consistent with the prominent cystic degeneration involving much of the lateral funiculus noted on the T2 sequence and histology. Compared with normal lateral funiculus white matter, the $D\parallel$ for chronic hemi-contusion was not statistically significantly different, while $D\perp$ remained significantly elevated ($p < 0.01$) and AI remained significantly depressed ($p < 0.01$).

Diffusion MRI marginal to injury epicenter distinguishes EB and contusion SCI at early and chronic phases

Values for $D\parallel$, $D\perp$, and AI measured in the ipsilateral lateral funiculus in regions without appreciable T2 signal abnormality marginal to the injury epicenter (3 mm and 6 mm cranial and caudal) during early and chronic time-points are summarized in Tables 2 and 3 and Figures 4 and 7. Of note, no diffusion parameters marginal to the EB injury epicenter were significantly different from normal white matter during the acute or chronic phases. At the early phase of hemi-contusion injury, AI and $D\parallel$ in the ipsilateral lateral funiculus were significantly decreased at axial slices 3 mm cranial and 3 mm caudal to the injury epicenter while $D\perp$ was

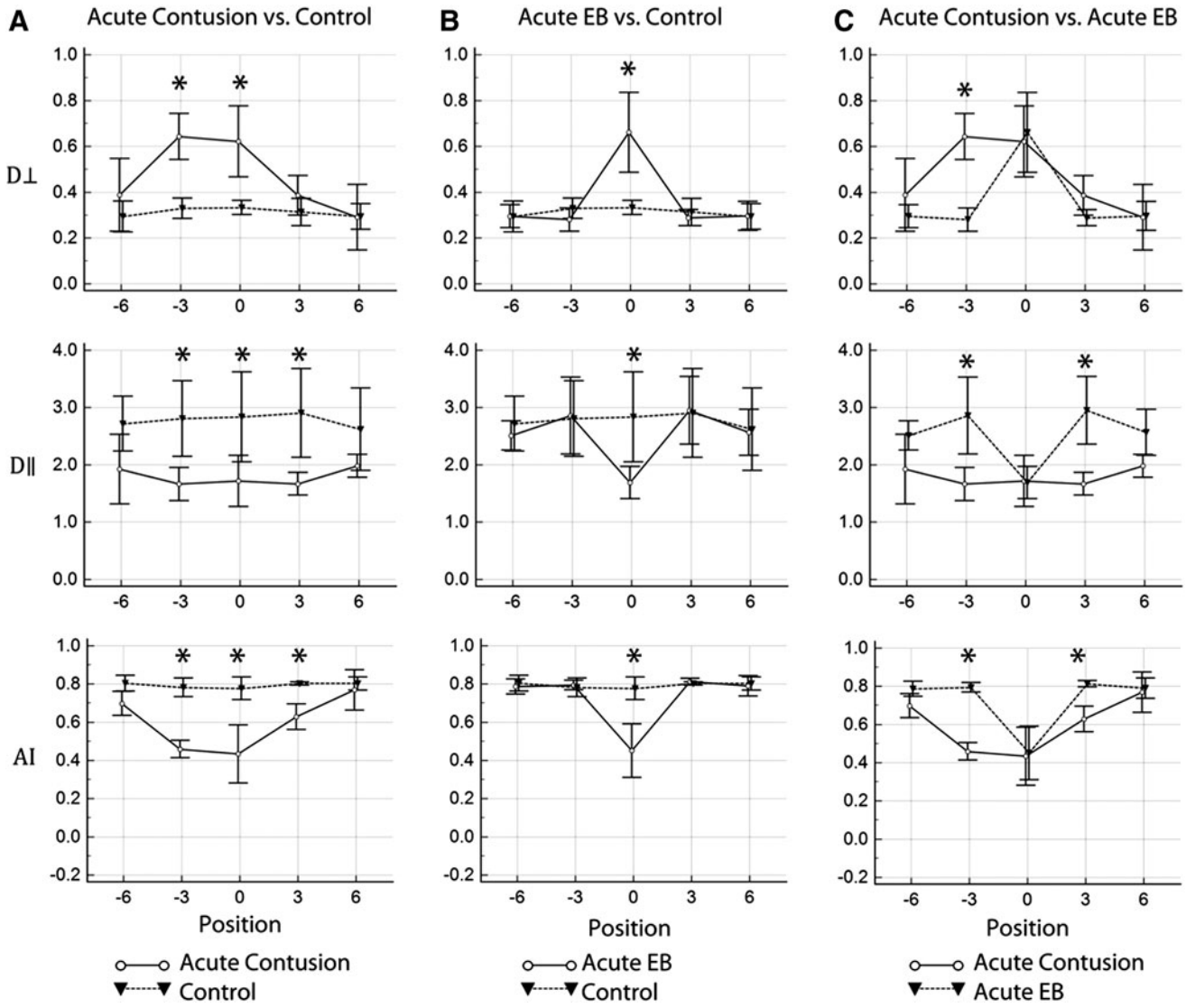

FIG. 4. Graphical representation of diffusion metrics in acute injury. D⊥, D‖, and AI values in the lateral funiculus of acute contusion versus control **(A)**, acute EB versus control **(B)**, and acute contusion versus EB **(C)**. The x-axis designates the craniacaudal region of spinal cord sampled with ''0'' representing the injury epicenter. Negative values (in mm) are caudal and positive values are cranial. * Indicates a statistically significant difference at the designated level. Units for D‖ and D⊥ values are cm^2*sec^{-1}. D‖, longitudinal apparent diffusion coefficient; D⊥, transverse apparent diffusion coefficient; AI, anisotropy index; EB, ethidium bromide.

elevated 3 mm caudal to the epicenter (Fig. 7). At the chronic time-point, craniocaudal asymmetry was apparent, with AI significantly reduced 6 mm and 3 mm caudal to the epicenter, while D⊥ was elevated 3 mm caudal. D‖ was elevated 3 mm caudal and 3 mm cranial to the epicenter in chronic hemi-contusion injury.

Discussion

In this study, we measured *in vivo* diffusion MRI values (D‖, D⊥, and AI) in the cervical spinal cord lateral funiculus after focal EB-induced demyelination and severe hemi-contusion SCI at both early and chronic time-points. During the early period, EB-induced chemical demyelination resulted in uniform demyelination with preservation of intact axons. Compared with controls, we observed significant elevation in D⊥ in EB lesions, as would be predicted by previous literature associating demyelination with increased D⊥.[11,12,14,15] Interestingly, we also observed concomitant reductions in D‖ in early EB lesions, despite quantitative histological evidence for uniform axonal preservation. Importantly, the degree of D⊥ and D‖ alterations within the EB demyelination epicenter at 7 dpi were not significantly different from those measured at the epicenter of early severe contusion injuries, where most axons and myelin are completely and irreversibly injured. This finding was unexpected in light of considerable prior literature suggesting D‖ and D⊥ may serve as biomarkers of axonal injury and demyelination respectively.[12,15,31] Specifically, we initially hypothesized that elevations in D⊥ with relative preservation of D‖ would be seen with EB demyelination, while concurrent hindered D‖ and elevated D⊥ would characterize severe contusion injury at the early post-injury time period.

Consistent with our findings, a growing body of literature has called into question the specificity of directional MRI diffusion metrics with respect to white matter microstructural alterations.[7,20,32] For example, in a contusive model of SCI in rats,

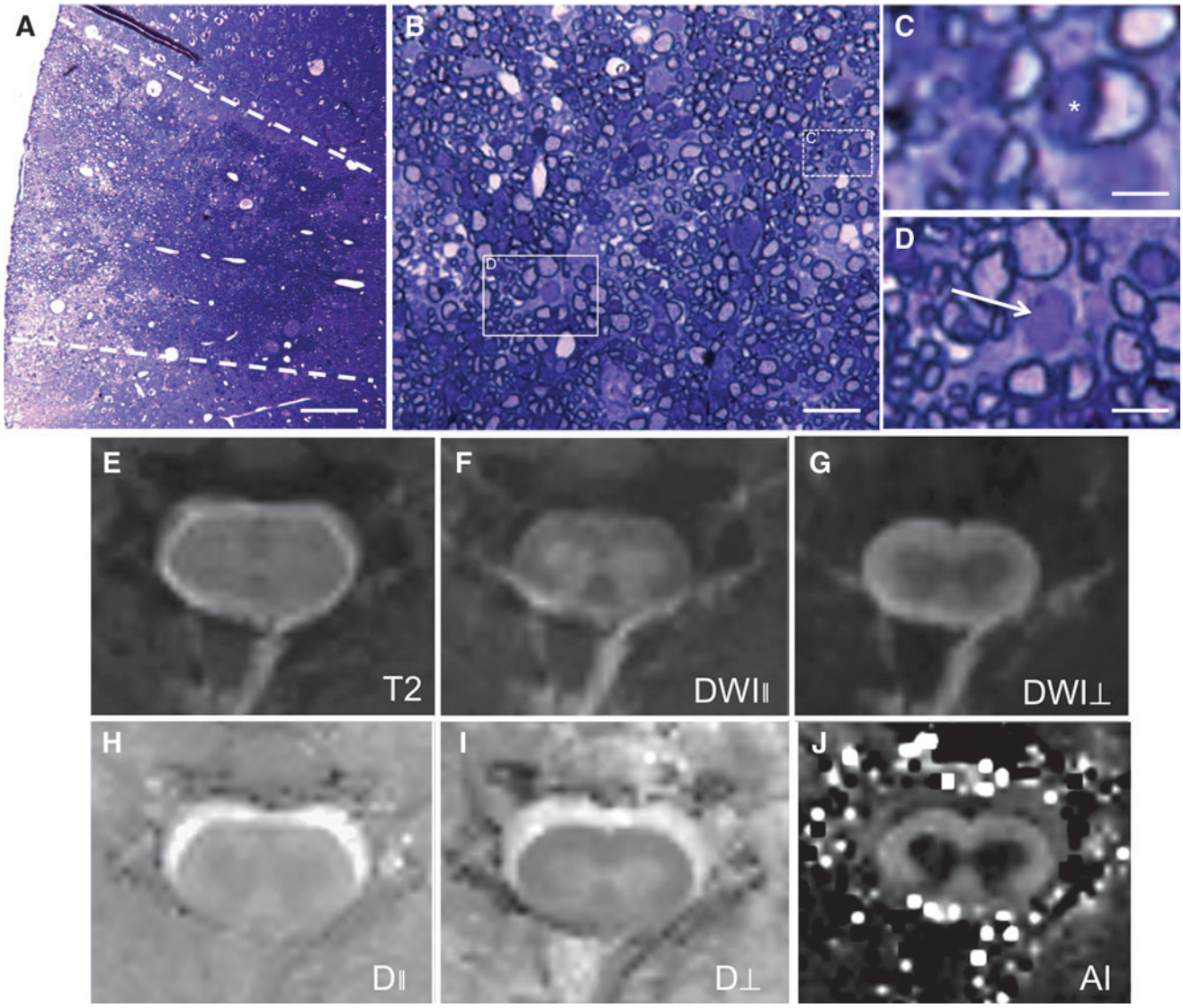

FIG. 5. Histology and magnetic resonance imaging of remyelinated chronic EB lesion. Low **(A)**, medium **(B)**, and high (**C** and **D**) magnification views of a toluidine-blue stained semi-thin section at the epicenter of a representative chronic EB lesion shows the characteristic heterogeneous myelin staining related to endogenous remyelination by a combination of Schwann cells (darker stain with thicker myelin ring) and oligodendrocytes. A high magnification view of a cluster of remyelinating Schwann cells (C) reveals the characteristic signet ring morphology. In D, a high magnification view of a remyelinating oligodendrocyte is shown (white arrow). Axial T2-weighted **(E)**, DWI-$\|$ **(F)**, DWI-$\perp$ **(G)**, D$\|$ **(H)**, D$\perp$ **(I),** and AI map **(J)** do not reveal any residual focal abnormality at the EB injection site. Post-operative changes related to laminectomy at the plane of imaging is noted dorsally. White solid line rectangle in B corresponds to panel C and white dashed line rectangle in B corresponds to panel D. EB, ethidium bromide; DWI-$\|$, longitudinal diffusion-weighted image; DWI-$\perp$, transverse diffusion-weighted image; D$\|$, longitudinal apparent diffusion coefficient; D$\perp$, transverse apparent diffusion coefficient; AI, anisotropy index. Scale bar = 250 μm in A, 15 μm in B, 3 μm in C and 5 μm in D. Color image is available online at www.liebertpub.com/neu

Sundberg and colleagues were unable to establish DTI correlates with specific pathologic changes.[7] In human multiple sclerosis lesions, Klawaiter and colleagues reported increased D$\perp$ as a surrogate marker for demyelination, but this metric also was elevated with axonal injury, thus limiting its pathologic specificity.[33] A detailed and rigorous longitudinal analysis of DTI parameters and histologic measures in cuprizone-induced demyelination of the corpus callosum revealed complex interplay between inflammatory cellular infiltrate, acute axonal injury, astrogliosis, and demyelination.[20] These pathologic changes all contribute as overlapping factors to consider with respect to alterations in water diffusion when probed with standard diffusion MRI models,[20] thus confounding the unique contributions from axonal injury and myelin disruption. Present data adds to this growing literature, highlighting the limited specificity of directional diffusion values for interrogation of axon injury and demyelination. This limitation is increasingly important to emphasize as specific pathologic white matter changes are now commonly implied in human studies based solely upon directional diffusion metrics in the absence of ground truth pathologic validation.[34–40]

Although EB demyelination has been extensively utilized to study mechanisms of endogenous and graft-mediated remyelination,[23,41–43] to our knowledge this is the first study to examine MRI features of EB-induced injury. EB demyelination does not precisely replicate

Table 3. Chronic Injury Diffusion Metrics

		Chronic injury (65 dpi)					
					p *value from post-ANOVA pairwise comparisons*		
Region	*Measure*	*Chronic contusion (CC)*	*Chronic ethidium bromide (CEB)*	*Control (C)*	*CC vs. C*	*CEB vs. C*	*CC vs. CEB*
Cranial 6	$D_{\perp}$	0.289 ± 0.067	0.296 ± 0.083	0.294 ± 0.056	NS	NS	NS
	$D_{\parallel}$	1.849 ± 0.372	2.302 ± 0.232	2.620 ± 0.719	NS	NS	NS
	AI	0.724 ± 0.077	0.772 ± 0.062	0.802 ± 0.034	NS	NS	NS
Cranial 3	$D_{\perp}$	0.353 ± 0.109	0.267 ± 0.110	0.313 ± 0.060	NS	NS	NS
	$D_{\parallel}$	1.787 ± 0.248	2.325 ± 0.323	2.905 ± 0.774	<0.05	>0.05	>0.05
	AI	0.665 ± 0.124	0.800 ± 0.052	0.802 ± 0.009	>0.05	>0.05	>0.05
Epicenter	$D_{\perp}$	2.215 ± 0.904	0.274 ± 0.067	0.334 ± 0.030	<0.01	>0.05	<0.01
	$D_{\parallel}$	2.674 ± 0.220	2.445 ± 0.461	2.837 ± 0.782	>0.05	>0.05	>0.05
	AI	0.122 ± 0.184	0.804 ± 0.029	0.777 ± 0.060	<0.01	>0.05	<0.01
Caudal 3	$D_{\perp}$	0.572 ± 0.086	0.303 ± 0.109	0.329 ± 0.044	<0.01	>0.05	<0.01
	$D_{\parallel}$	1.519 ± 0.199	2.167 ± 0.057	2.808 ± 0.659	<0.01	>0.05	>0.05
	AI	0.453 ± 0.050	0.757 ± 0.078	0.782 ± 0.049	<0.01	>0.05	<0.01
Caudal 6	$D_{\perp}$	0.441 ± 0.089	0.308 ± 0.066	0.210 ± 0.068	NS	NS	NS
	$D_{\parallel}$	1.900 ± 0.313	2.616 ± 0.627	2.719 ± 0.481	NS	NS	NS
	AI	0.620 ± 0.080	0.783 ± 0.054	0.788 ± 0.041	<0.01	>0.05	<0.01

NS = non-significant ANOVA that did not go on to pairwise comparisons with a Tukey-Kramer *post hoc* test. dpi, days post-injury; ANOVA, analysis of variance; $D\perp$, magnetic resonance imaging (MRI)–derived measurements of water diffusion perpendicular to white matter tracts; $D\parallel$, MRI-derived measurements of water diffusion parallel to white matter tracts; AI, anisotropy index.

any known clinical disease; however, it is ideally suited for evaluating diffusion MRI correlates of myelin pathology *in vivo* in the absence of significant secondary axonal injury or primary inflammatory response. In addition to preserving axons, EB lesions are focal, with relatively homogenous fields of denuded axons and a highly predictable temporal course of demyelination and subsequent endogenous remyelination.[24] Consistent with previous studies, we observed no appreciable pathologic changes in demyelinated axons as a result of EB demyelination. This is in contrast to inflammatory, ischemic, and traumatic injury models, which have previously been used to correlate diffusion MRI parameters with myelin pathology.

For example, coexistent axonal pathology, demyelination, astrogliosis, and large inflammatory cellular infiltrates confound interpretation of DTI parameters in cuprizone,[20] experimental autoimmune encephalomyelitis (EAE),[44] and contusive[7,14] injury models. Even in the absence of confounding acute axon pathology, astrogliosis, or primary inflammatory response with EB demyelination, the degree of hindered $D\parallel$ in acute EB lesions was indistinguishable from that observed with severe contusion injury. Thus, pathologic features of EB demyelination do reduce $D\parallel$ independent of axonal disruption. Leading potential histologic correlates for this observed reduction in $D\parallel$ in the EB lesion at the early phase of injury include accumulation of extracellular myelin debris and slight increased cellularity related to phagocytic macrophages known to clear myelin debris within the EB lesion. Elevations in $D\perp$ in acute EB lesions also were indistinguishable in degree from acute severe contusion injury. This finding is less surprising as demyelination is a prominent component of both injury models and elevated $D\perp$ would be predicted by many prior studies.[15,45] Some component of vasogenic edema in both injury models also likely contributes to observed elevations in $D\perp$.

Recent studies suggest that more advanced diffusion analysis techniques, including diffusion basis spectrum imaging (DBSI), may in part overcome some of these limitations.[21,46,47] DBSI models water diffusion as a combination of anisotropic and isotropic diffusion tensors.[21] The isotropic tensor component theoretically accounts for diffusion effects of inflammation, tissue loss, and vasogenic edema. When this isotropic tensor component is removed, the specific contributions of axonopathy and myelinopathy may be more accurately derived with DBSI-derived diffusivity measurements.[21,46,47] However, DBSI requires the sampling of a high number of diffusion directions with relatively long imaging times and has not yet been validated for *in vivo* spinal cord imaging.

Diffusion MRI identifies marginal pathology in contusion SCI but not EB demyelination at 7 dpi

Another important finding from the current study is that significant alterations in $D\parallel$, $D\perp$, and AI were evident in spinal cord normal-appearing white matter (NAWM) on T2-weighted images at sites cranial and caudal to the contusion injury epicenter, whereas no diffusion alterations were seen in corresponding regions following EB demyelination. The absence of detectable alterations in diffusion metrics adjacent to the epicenter of acute EB demyelination is not surprising given the focality of this injury and absence of histologic abnormality marginal to the epicenter. Our finding of diffusion changes cranial and caudal to the severe contusion injury epicenter in regions of NAWM on T2-weighted images is consistent with results from several recent studies.[7,19,44,48,49] Craniocaudal asymmetry with decreased AI more extensively seen caudal to the epicenter in chronic SCI also is consistent with prior studies examining the lateral funiculus in SCI, and likely relates to a relative predominance of descending fibers in the ROI selected for analysis.[13,14,50] Current results further highlight the value of a comprehensive spatial analysis for interrogation of white matter diffusion metrics along the craniocaudal axis of the spinal cord. In the setting of focal lesions, such as traumatic SCI or compressive myelopathy, a holistic evaluation of the spinal cord white matter that is not limited to the injury epicenter may help distinguish between axon-sparing and axonopathic injury, and perhaps better assess the severity of injury, compared with evaluation limited to the injury epicenter.

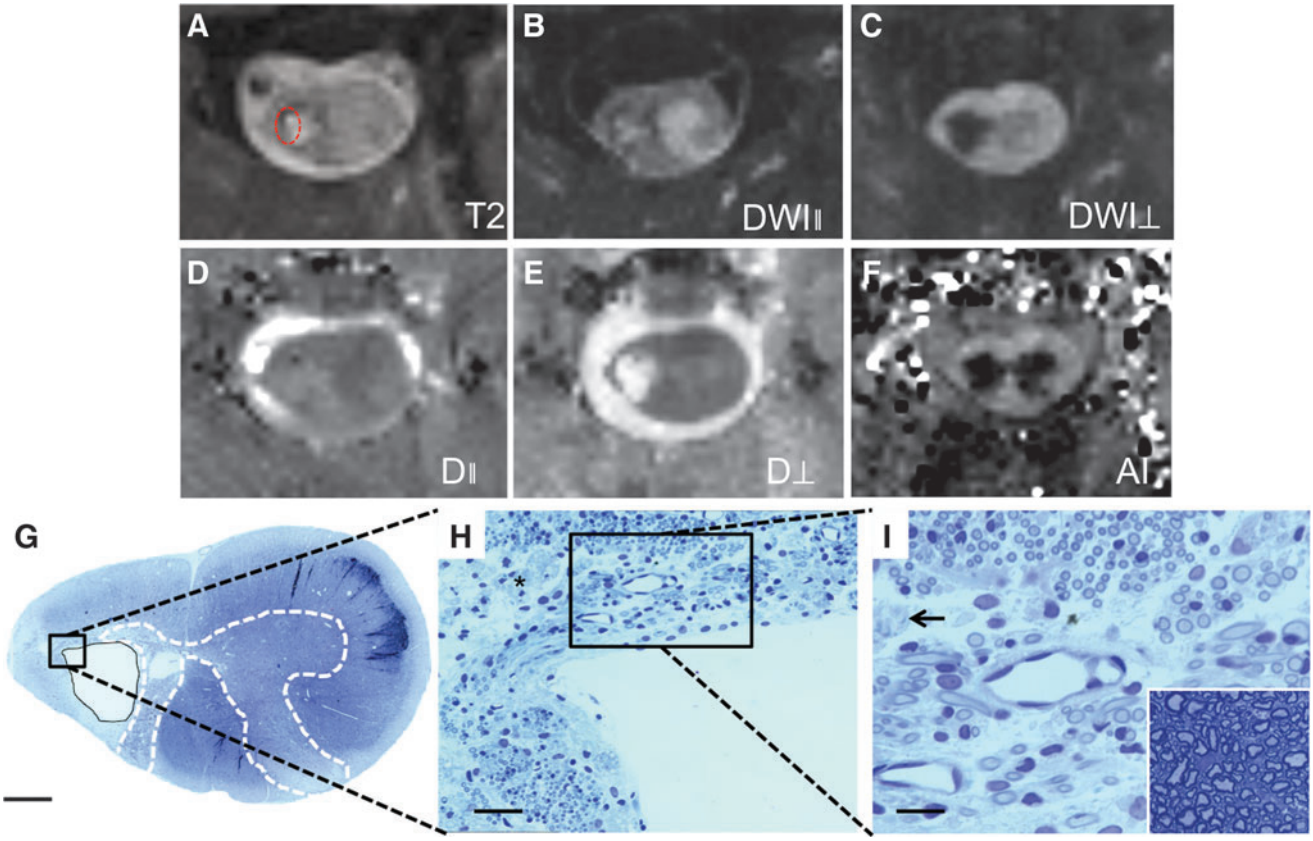

FIG. 6. Magnetic resonance imaging (MRI) and histology of chronic hemi-contusion spinal cord injuyr. **(A)** Cystic myelomalacia of the lateral funiculus is evidenced by a dominant T2 hyperintense cavity seen on axial T2-weighted image. Associated diffusion alterations are seen on the DWI-∥ **(B)**, DWI-⊥ **(C)**, D∥ **(D)**, D⊥ **(E),** and AI map **(F)** images at the injury epicenter. The cavitary margins exhibit T2-hypointense signal consistent with chronic blood products and fibrous scar. Red dashed oval in A approximates the ROI selected for diffusion MRI analysis in chronic contusion injuries, revealing significantly elevated D⊥ and significantly reduced D∥ and AI values. Low magnification image **(G)** of the entire transverse extent of the cord from a representative toluidine blue–stained section demonstrates the pathologic correlate for MRI findings. Gray irregular oval outlines the cystic cavity margins and dashed white lines outline approximate gray matter boundaries in G. Medium 40× **(H)** and high 100× **(I)** magnification images centered along the ventrolateral margin of the cystic cavity at the injury epicenter reveal sparcely distributed remyelinated axons (many of which are remyelinated by Schwann cells), fibrous interstitial tissue, and scattered macrophages (black arrow in I). For reference, right lower inset in panel I shows normal axonal density and myelin thickness in the contralateral ventrolateral funiculus. Black rectangles in G and H correspond to ROI selected for progressive higher magnificantion panels H and I respectively. DWI-∥, longitudinal diffusion-weighted image; DWI-⊥, transverse diffusion-weighted image; AI, anisotropy index; D⊥, transverse apparent diffusion coefficient; D∥, longitudinal apparent diffusion coefficient; ROI, region of interest. Scale bar = 300 μm in G, 15 μm in H, and 5 μm I. Color image is available online at www.liebertpub.com/neu

Diffusion abnormalities resolve with remyelination of EB lesions but persist following contusion

Endogenous remyelination of EB lesions occurs completely within approximately 4 weeks of injury by a combination of both oligodendrocytes and Schwann cells.[24] We observed complete resolution of T2 signal abnormality and diffusion parameters following endogenous remyelination of EB lesions after 65 days. No myelomalacia was noted in chronic EB animals. In contrast, chronic contusion injuries were associated with cystic cavitation at the injury epicenter, with persistent abnormalities in directional diffusion values at the epicenter and in NAWM of the lateral funiculus cranial and caudal to the epicenter. At the contusion injury epicenter, the apparent ''normalization'' of D∥ that we observed at chronic time-points has been similarly observed in a prior study.[7] In our experience, this finding does not reflect recovery of tissue microarchitecture or axonal regeneration, but rather results from near isotropic diffusion of water within the predominantly cystic lesion core that approximates longitudinal diffusion seen in intact healthy white matter where diffusion paralleling axon bundles is relatively unhindered. This observation further highlights the importance of understanding the pathologic context for interpretation of directional diffusion values.

Study limitations

A potential limitation to the current study was the use of directional ADC values (D∥ and D⊥) in lieu of DTI-derived directional diffusivities ($\lambda\|$ and $\lambda\perp$). DTI-dervied $\lambda\|$ and $\lambda\perp$ are rotationally invariant scalar metrics and independent of animal positioning relative to the magnetic field reference frame. Instead, we relied on directional ADC values, which are dependent on alignment of the spinal cord within the magnetic field reference frame. Great care was taken to ensure that the primary spinal cord axes were physically aligned with the magnetic field reference frame as has been previously described.[3,51,52] Tu and colleagues have validated this

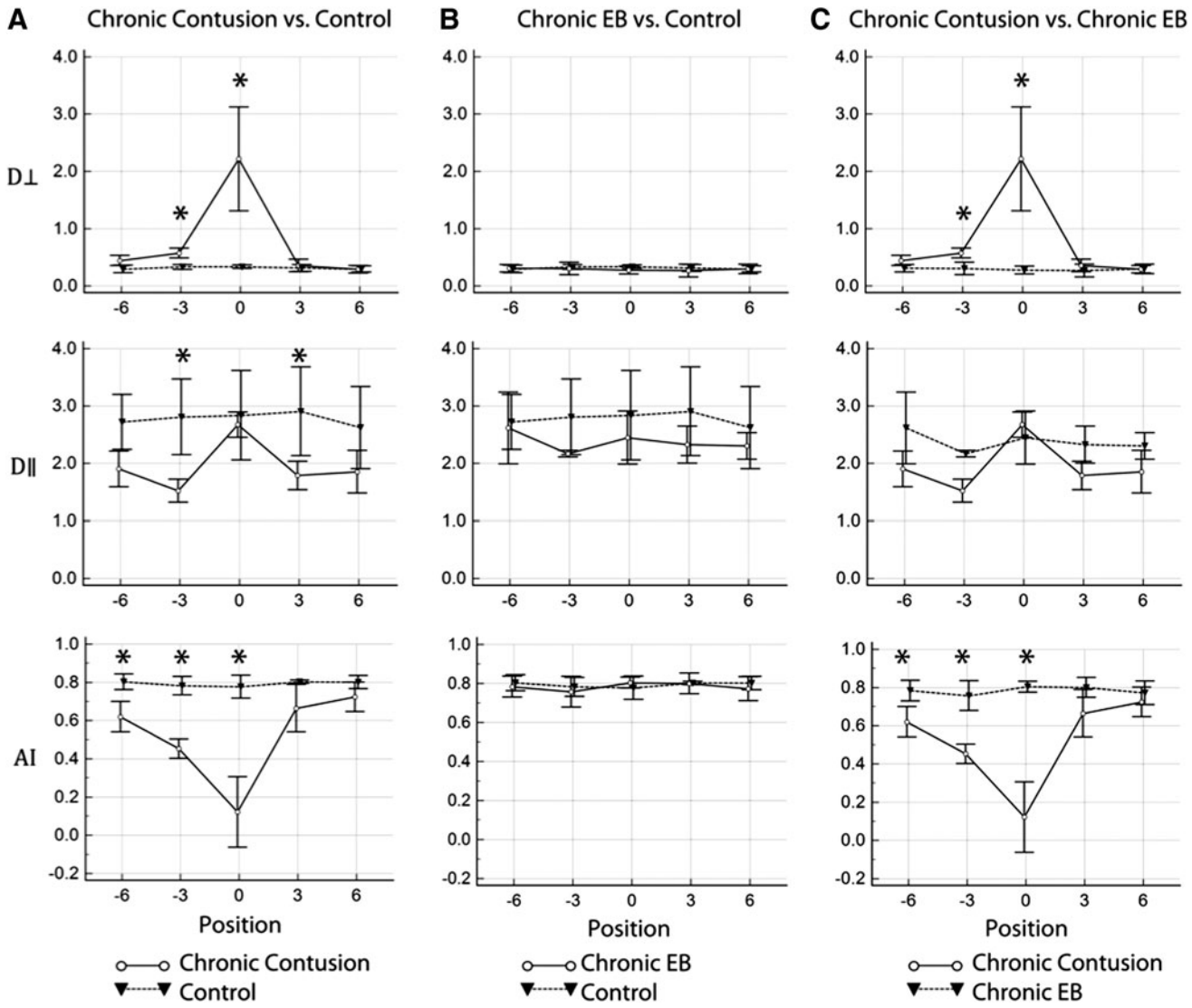

FIG. 7. Graphical representation of diffusion metrics in chronic injury. D⊥, D‖, and AI values in the lateral funiculus of chronic contusion versus control **(A)**, chronic EB versus control **(B)**, and chronic contusion versus chronic EB **(C)** injury. The x-axis designates the craniocaudal region of spinal cord sampled with ''0'' representing the injury epicenter. Negative values (in mm) are caudal and positive values are cranial. * Indicates a statistically significant difference at the designated level. Units for D‖ and D⊥ values are cm^2*sec^{-1}. D‖, longitudinal apparent diffusion coefficient; D⊥, transverse apparent diffusion coefficient; AI, anisotropy index; EB, ethidium bromide.

approach for evaluation of spinal cord white matter.[26] Importantly, prior simulation and *in vivo* studies have suggested that white matter pathology can fictitiously alter the direction of the principal diffusion tensor eigenvector with respect to underlying white matter tracts, thereby limiting the utility of diffusion tensor–derived diffusivities as biomarkers of structural abnormality following injury.[32] Directional ADC values oriented parallel and perpendicular to the known spinal cord long axis may better reflect structural white matter alterations of ascending and descending long tracts, although this was not explicitly tested in the current study. Our *in vivo* measurements of normal rodent spinal cord white matter D‖ and D⊥ are in line with previously reported values for $\lambda\|$ and $\lambda\perp$.[52]

Conclusion

In the present study, we show that when analysis is focused at the injury epicenter, directional diffusion MRI values (D‖ and D⊥) at the early stage of injury do not reliably distinguish a relatively pure axon sparing demyelinating injury from a severe hemi-contusion injury, which ablates most axons and myelin. Present data build upon recent studies showing that many factors, in addition to axon injury and demyelination, contribute to alterations in water diffusivity as measured with conventional diffusion MRI techniques and confound the specificity of directional diffusion measurements after injury,[20,21,46] even in a relatively pure model of axon-sparing chemical demyelination. We advise caution in ascribing particular microstructural alterations to diffusion MRI-derived directional diffusion metrics in the absence of pathologic correlation, a practice that has permeated the clinical literature over the past decade. Further, diffusion measurements of NAWM cranial and caudal to the acute injury epicenter are helpful for characterizing the nature of spinal cord white matter injury. Current results further validate the utilization of a longitudinal interrogation of white matter diffusion metrics along the craniocaudal axis of the spinal cord for

distinction between axon-sparing and axonopathic white matter injury in favor of analysis limited to the injury epicenter.

Acknowledgments

We thank Amity Lin for excellent technical expertise and contributions to animal surgery and tissue processing. We also thank Xiaokui Ma, M.D., for her excellent assistance with histopathologic processing of spinal cord tissue. This work was supported by NIH National Institute of Neurological Disorders and Stroke grant #R01NS038079 (MSB, JCB), #R21-AG032518 (MSB, JCB) and Department of Defense grant CDMRP SCIRP 120559 (W81XWH-13-1-0297; MSB and JCB).

Author Disclosure Statement

JFT is a member of the data monitoring committee for StemCells, Inc. For the other authors, no competing financial interests exist.

References

1. Bozzo, A., Marcoux, J., Radhakrishna, M., Pelletier, J., and Goulet, B. (2011). The role of magnetic resonance imaging in the management of acute spinal cord injury. J. Neurotrauma 28, 1401–1411.
2. Le Bihan, D., Mangin, J.F., Poupon, C., Clark, C.A., Pappata, S., Molko, N., and Chabriat, H. (2001). Diffusion tensor imaging: concepts and applications. J. Magn. Reson. Imaging 13, 534–546.
3. Ford, J.C., Hackney, D.B., Alsop, D.C., Jara, H., Joseph, P.M., Hand, C.M., and Black, P. (1994). MRI characterization of diffusion coefficients in a rat spinal cord injury model. Magn. Reson. Med. 31, 488–494.
4. Schwartz, E.D., Cooper, E.T., Fan, Y., Jawad, A.F., Chin, C.L., Nissanov, J., and Hackney, D.B. (2005). MRI diffusion coefficients in spinal cord correlate with axon morphometry. Neuroreport 16, 73–76.
5. Schwartz, E.D. and Hackney, D.B. (2003). Diffusion-weighted MRI and the evaluation of spinal cord axonal integrity following injury and treatment. Exp. Neurol. 184, 570–589.
6. Ford, J.C., Hackney, D.B., Joseph, P.M., Phelan, M., Alsop, D.C., Tabor, S.L., Hand, C.M., Markowitz, R.S., and Black, P. (1994). A method for in vivo high resolution MRI of rat spinal cord injury. Magn. Reson. Med. 31, 218–223.
7. Sundberg, L.M., Herrera, J.J., and Narayana, P.A. (2010). In vivo longitudinal MRI and behavioral studies in experimental spinal cord injury. J. Neurotrauma 27, 1753–1767.
8. Loy, D.N., Kim, J.H., Xie, M., Schmidt, R.E., Trinkaus, K., and Song, S.K. (2007). Diffusion tensor imaging predicts hyperacute spinal cord injury severity. J. Neurotrauma 24, 979–990.
9. Budde, M.D., Kim, J.H., Liang, H.F., Russell, J.H., Cross, A.H., and Song, S.K. (2008). Axonal injury detected by in vivo diffusion tensor imaging correlates with neurological disability in a mouse model of multiple sclerosis. NMR Biomed, 21, 589–597.
10. Song, B., Meng, F., Yan, X., Guo, J., and Zhang, G. (2003). Cerebral ischemia immediately increases serine phosphorylation of the synaptic RAS-GTPase activating protein SynGAP by calcium/calmodulin-dependent protein kinase II alpha in hippocampus of rats. Neurosci. Lett. 349, 183–186.
11. Song, S.K., Sun, S.W., Ramsbottom, M.J., Chang, C., Russell, J., and Cross, A.H. (2002). Dysmyelination revealed through MRI as increased radial (but unchanged axial) diffusion of water. NeuroImage 17, 1429–1436.
12. Song, S.K., Yoshino, J., Le, T.Q., Lin, S.J., Sun, S.W., Cross, A.H., and Armstrong, R.C. (2005). Demyelination increases radial diffusivity in corpus callosum of mouse brain. NeuroImage 26, 132–140.
13. Kim, J.H., Loy, D.N., Liang, H.F., Trinkaus, K., Schmidt, R.E., and Song, S.K. (2007). Noninvasive diffusion tensor imaging of evolving white matter pathology in a mouse model of acute spinal cord injury. Magn. Reson. Med. 58, 253–260.
14. Brennan, F.H., Cowin, G.J., Kurniawan, N.D., and Ruitenberg, M.J. (2013). Longitudinal assessment of white matter pathology in the injured mouse spinal cord through ultra-high field (16.4 T) in vivo diffusion tensor imaging. NeuroImage 82, 574–585.
15. Song, S.K., Sun, S.W., Ju, W.K., Lin, S.J., Cross, A.H., and Neufeld, A.H. (2003). Diffusion tensor imaging detects and differentiates axon and myelin degeneration in mouse optic nerve after retinal ischemia. NeuroImage 20, 1714–1722.
16. Budde, M.D., Kim, J.H., Liang, H.F., Schmidt, R.E., Russell, J.H., Cross, A.H., and Song, S.K. (2007). Toward accurate diagnosis of white matter pathology using diffusion tensor imaging. Magn. Reson. Med. 57, 688–695.
17. Budde, M.D., Xie, M., Cross, A.H., and Song, S.K. (2009). Axial diffusivity is the primary correlate of axonal injury in the experimental autoimmune encephalomyelitis spinal cord: a quantitative pixelwise analysis. J. Neurosci. 29, 2805–2813.
18. Kim, J.H., Loy, D.N., Wang, Q., Budde, M.D., Schmidt, R.E., Trinkaus, K., and Song, S.K. (2010). Diffusion tensor imaging at 3 hours after traumatic spinal cord injury predicts long-term locomotor recovery. J. Neurotrauma 27, 587–598.
19. Kozlowski, P., Rosicka, P., Liu, J., Yung, A.C., and Tetzlaff, W. (2014). In vivo longitudinal Myelin Water Imaging in rat spinal cord following dorsal column transection injury. Magn. Reson. Imaging 32, 250–258.
20. Xie, M., Tobin, J.E., Budde, M.D., Chen, C.I., Trinkaus, K., Cross, A.H., McDaniel, D.P., Song, S.K., and Armstrong, R.C. (2010). Rostrocaudal analysis of corpus callosum demyelination and axon damage across disease stages refines diffusion tensor imaging correlations with pathological features. J. Neuropathol. Exp. Neurol. 69, 704–716.
21. Wang, Y., Wang, Q., Haldar, J.P., Yeh, F.C., Xie, M., Sun, P., Tu, T.W., Trinkaus, K., Klein, R.S., Cross, A.H., and Song, S.K. (2011). Quantification of increased cellularity during inflammatory demyelination. Brain 134, 3590–3601.
22. Blakemore, W.F. (1982). Ethidium bromide induced demyelination in the spinal cord of the cat. Neuropathol. Appl. Neurobiol. 8, 365–375.
23. Blakemore, W.F. and Franklin, R.J. (2008). Remyelination in experimental models of toxin-induced demyelination. Curr. Top. Microbial. Immunol. 318, 193–212.
24. Talbott, J.F., Loy, D.N., Liu, Y., Qiu, M.S., Bunge, M.B., Rao, M.S., and Whittemore, S.R. (2005). Endogenous Nkx2.2+/Olig2+ oligodendrocyte precursor cells fail to remyelinate the demyelinated adult rat spinal cord in the absence of astrocytes. Exp. Neurol. 192, 11–24.
25. Talbott, J.F., Cao, Q., Enzmann, G.U., Benton, R.L., Achim, V., Cheng, X.X., Mills, M.D., Rao, M.S., and Whittemore, S.R. (2006). Schwann cell-like differentiation by adult oligodendrocyte precursor cells following engraftment into the demyelinated spinal cord is BMP-dependent. Glia 54, 147–159.
26. Tu, T.W., Kim, J.H., Wang, J., and Song, S.K. (2010). Full tensor diffusion imaging is not required to assess the white-matter integrity in mouse contusion spinal cord injury. J. Neurotrauma 27, 253–262.
27. Mihai, G., Nout, Y.S., Tovar, C.A., Miller, B.A., Schmalbrock, P., Bresnahan, J.C., and Beattie, M.S. (2008). Longitudinal comparison of two severities of unilateral cervical spinal cord injury using magnetic resonance imaging in rats. J. Neurotrauma 25, 1–18.
28. Nout, Y.S., Mihai, G., Tovar, C.A., Schmalbrock, P., Bresnahan, J.C., and Beattie, M.S. (2009). Hypertonic saline attenuates cord swelling and edema in experimental spinal cord injury: a study utilizing magnetic resonance imaging. Crit. Care Med. 37, 2160–2166.
29. Beattie, M.S., Bresnahan, J.C., Komon, J., Tovar, C.A., Van Meter, M., Anderson, D.K., Faden, A.I., Hsu, C.Y., Noble, L.J., Salzman, S., and Young, W. (1997). Endogenous repair after spinal cord contusion injuries in the rat. Exp. Neurol. 148, 453–463.
30. Gensel, J.C., Tovar, C.A., Hamers, F.P., Deibert, R.J., Beattie, M.S., and Bresnahan, J.C. (2006). Behavioral and histological characterization of unilateral cervical spinal cord contusion injury in rats. J. Neurotrauma 23, 36–54.
31. Song, S.K., Qu, Z., Garabedian, E.M., Gordon, J.I., Milbrandt, J., and Ackerman, J.J. (2002). Improved magnetic resonance imaging detection of prostate cancer in a transgenic mouse model. Cancer Res. 62, 1555–1558.
32. Wheeler-Kingshott, C.A. and Cercignani, M. (2009). About ''axial'' and ''radial'' diffusivities. Magn. Reson. Med. 61, 1255–1260.
33. Klawiter, E.C., Schmidt, R.E., Trinkaus, K., Liang, H.F., Budde, M.D., Naismith, R.T., Song, S.K., Cross, A.H., and Benzinger, T.L. (2011). Radial diffusivity predicts demyelination in ex vivo multiple sclerosis spinal cords. NeuroImage 55, 1454–1460.
34. Oguz, K.K., Haliloglu, G., Temucin, C., Gocmen, R., Has, A.C., Doerschner, K., Dolgun, A., and Alikasifoglu, M. (2013). Assessment of whole-brain white matter by DTI in autosomal recessive spastic ataxia of Charlevoix-Saguenay. A.J.N.R. Am.J. Neuroradiol. 34, 1952–1957.
35. Lin, W.C., Chou, K.H., Chen, C.L., Chen, H.L., Lu, C.H., Li, S.H., Huang, C.C., Lin, C.P., and Cheng, Y.F. (2014). Longitudinal brain

white matter alterations in minimal hepatic encephalopathy before and after liver transplantation. PloS One 9, e105887.
36. Lobsien, D., Ettrich, B., Sotiriou, K., Classen, J., Then Bergh, F., and Hoffmann, K.T. (2014). Whole-brain diffusion tensor imaging in correlation to visual-evoked potentials in multiple sclerosis: a tract-based spatial statistics analysis. A.J.N.R. Am. J. Neuroradiol. 35, 2076–2081.
37. Bonzano, L., Tacchino, A., Brichetto, G., Roccatagliata, L., Dessypris, A., Feraco, P., Lopes De Carvalho, M.L., Battaglia, M.A., Mancardi, G.L., and Bove, M. (2014). Upper limb motor rehabilitation impacts white matter microstructure in multiple sclerosis. NeuroImage 90, 107–116.
38. Lawrence, A.J., Patel, B., Morris, R.G., MacKinnon, A.D., Rich, P.M., Barrick, T.R., and Markus, H.S. (2013). Mechanisms of cognitive impairment in cerebral small vessel disease: multimodal MRI results from the St George's cognition and neuroimaging in stroke (SCANS) study. PloS One 8, e61014.
39. Aung, W.Y., Mar, S., and Benzinger, T.L. (2013). Diffusion tensor MRI as a biomarker in axonal and myelin damage. Imaging Med. 5, 427–440.
40. Gupta, N., Henry, R.G., Strober, J., Kang, S.M., Lim, D.A., Bucci, M., Caverzasi, E., Gaetano, L., Mandelli, M.L., Ryan, T., Perry, R., Farrell, J., Jeremy, R.J., Ulman, M., Huhn, S.L., Barkovich, A.J., and Rowitch, D.H. (2012). Neural stem cell engraftment and myelination in the human brain. Sci. Transl. Med. 4, 155ra137.
41. Crang, A.J., Franklin, R.J., Blakemore, W.F., Noble, M., Barnett, S.C., Groves, A., Trotter, J., and Schachner, M. (1992). The differentiation of glial cell progenitor populations following transplantation into non-repairing central nervous system glial lesions in adult animals. J. Neuroimmunol. 40, 243–253.
42. Blakemore, W.F., Crang, A.J., and Franklin, R.J. (1990). Transplantation of glial cell cultures into areas of demyelination in the adult CNS. Prog. Brain Res. 82, 225–232.
43. Talbott, J.F., Cao, Q., Bertram, J., Nkansah, M., Benton, R.L., Lavik, E., and Whittemore, S.R. (2007). CNTF promotes the survival and differentiation of adult spinal cord-derived oligodendrocyte precursor cells in vitro but fails to promote remyelination in vivo. Exp. Neurol. 204, 485–489.
44. DeBoy, C.A., Zhang, J., Dike, S., Shats, I., Jones, M., Reich, D.S., Mori, S., Nguyen, T., Rothstein, B., Miller, R.H., Griffin, J.T., Kerr, D.A., and Calabresi, P.A. (2007). High resolution diffusion tensor imaging of axonal damage in focal inflammatory and demyelinating lesions in rat spinal cord. Brain 130, 2199–2210.
45. Sun, S.W., Song, S.K., Harms, M.P., Lin, S.J., Holtzman, D.M., Merchant, K.M., and Kotyk, J.J. (2005). Detection of age-dependent brain injury in a mouse model of brain amyloidosis associated with Alzheimer's disease using magnetic resonance diffusion tensor imaging. Exp. Neurol. 191, 77–85.
46. Chiang, C.W., Wang, Y., Sun, P., Lin, T.H., Trinkaus, K., Cross, A.H., and Song, S.K. (2014). Quantifying white matter tract diffusion parameters in the presence of increased extra-fiber cellularity and vasogenic edema. NeuroImage 101, 310–319.
47. Wang, X., Cusick, M.F., Wang, Y., Sun, P., Libbey, J.E., Trinkaus, K., Fujinami, R.S., and Song, S.K. (2014). Diffusion basis spectrum imaging detects and distinguishes coexisting subclinical inflammation, demyelination and axonal injury in experimental autoimmune encephalomyelitis mice. NMR Biomed. 27, 843–852.
48. Jirjis, M.B., Kurpad, S.N., and Schmit, B.D. (2013). Ex vivo diffusion tensor imaging of spinal cord injury in rats of varying degrees of severity. J. Neurotrauma 30, 1577–1586.
49. Kelley, B.J., Harel, N.Y., Kim, C.Y., Papademetris, X., Coman, D., Wang, X., Hasan, O., Kaufman, A., Globinsky, R., Staib, L.H., Cafferty, W.B., Hyder, F., and Strittmatter, S.M. (2014). Diffusion tensor imaging as a predictor of locomotor function after experimental spinal cord injury and recovery. J. Neurotrauma 31, 1362–1373.
50. Cohen-Adad, J., Leblond, H., Delivet-Mongrain, H., Martinez, M., Benali, H., and Rossignol, S. (2011). Wallerian degeneration after spinal cord lesions in cats detected with diffusion tensor imaging. NeuroImage 57, 1068–1076.
51. Ford, J.C., Hackney, D.B., Lavi, E., Phillips, M., and Patel, U. (1998). Dependence of apparent diffusion coefficients on axonal spacing, membrane permeability, and diffusion time in spinal cord white matter. J. Magn. Reson. Imaging 8, 775–782.
52. Ellingson, B.M., Kurpad, S.N., Li, S.J., and Schmit, B.D. (2008). In vivo diffusion tensor imaging of the rat spinal cord at 9.4T. J. Magn. Reson. Imaging 27, 634–642.

Address correspondence to:
Jason F. Talbott, MD, PhD
San Francisco General Hospital
Department of Radiology
1001 Potrero Avenue, Room 1X57C
San Francisco, CA 94110

E-mail: jason.talbott@ucsf.edu